available at www.sciencedirect.com

ScienceDirect

journal homepage: www.elsevier.com/locate/chnjc

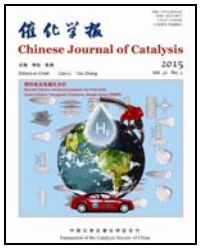

Article

A stable and active Ag_xS crystal preparation and its performance as photocatalyst

Pingjing Chang [a,b,c], Haiyang Cheng [a,b,#], Weiwei Lin [a,b], Xiaoru Li [a,b,c], Fengyu Zhao [a,b,*]

[a] *State Key Laboratory of Electroanalytical Chemistry, Changchun Institute of Applied Chemistry, Chinese Academy of Sciences, Changchun 130022, Jilin, China*

[b] *Laboratory of Green Chemistry and Process, Changchun Institute of Applied Chemistry, Chinese Academy of Sciences, Changchun 130022, Jilin, China*

[c] *University of Chinese Academy of Sciences, Beijing 100049, China*

ARTICLE INFO

Article history:
Received 23 November 2014
Accepted 8 January 2015
Published 20 April 2015

Keywords:
Silver sulfide
Visible light irradiation
Photocatalytic degradation
Organic pollutants
Band gap

ABSTRACT

Ag_xS crystals were synthesized via hydrothermal (Ag_xS-*H*) and *in situ* ion-exchange (Ag_xS-*IE*) methods. The samples were characterized by scanning electron microscopy, X-ray diffraction, ultraviolet-visible-near infrared absorption spectroscopy, N_2 adsorption-desorption, X-ray photoelectron spectroscopy and surface photovoltage measurements. The photocatalytic performance was investigated for the decomposition of methyl blue (MB) under visible light irradiation ($\lambda \geq 420$ nm). The Ag_xS-*H* had smaller particles, wider band gap and weaker recombination of photoinduced charges than Ag_xS-*IE*, resulting in a higher photocatalytic activity. Moreover, Ag_xS-*H* was stable, and could be reused five times without loss of photocatalytic activity. Additionally, a possible pathway for the photocatalytic degradation of MB over Ag_xS has been proposed, that MB was oxidized mainly by hydroxyl radicals and partly via electron holes generated in the Ag_xS. Ag_xS-*H* is an efficient photocatalyst and has great potential for the degradation of harmful organic dyes in wastewater.

1. Introduction

In recent years, rapid development of industry has led to large amounts of industrial wastewater containing organic pollutants such as dyes, pharmaceuticals, and even pathogenic microorganisms being released into water sources, resulting in increasing numbers of regions around the world suffering from water supply problems [1,2]. This has caused attention to be directed toward the treatment of wastewater containing textile dyes and other industrial dyestuffs, which include the largest groups of organic compounds that constitute an environmental problem. Many physical techniques, such as adsorption on activated carbon, ultrafiltration, reverse osmosis, coagulation by chemical agents, and ion exchange on synthetic adsorbent resins were used to remove dye pollutants [3]. However, these methods just transfer the dye pollutants from water to another phase, meaning the regeneration of the adsorbent materials and post-treatment of solid waste are necessary to prevent secondary pollution [4]. Conventional biological treatment methods are ineffective for the decolorization and degradation of highly aromatic dyes as they have been selected for their stability to these conditions [5–8]. Thus, advanced oxidation processes (AOPs) have attracted attention during the last decade because of their ability to deal with a broad range of dyes in aqueous systems, through processes such as the Fenton and photo-Fenton catalytic reaction [9–11], H_2O_2/UV processes [12,13] and TiO_2 mediated photocatalysis [14–18]. Among the AOPs, photocatalysis has received increasing attention [19–23],

* Corresponding author. Tel/Fax: +86-431-85262410; E-mail: zhaofy@ciac.ac.cn
# Corresponding author. Tel/Fax: +86-431-85262454; E-mail: hycyl@ciac.ac.cn
This work was supported by the National Natural Science Foundation of China (21273222).
DOI: 10.1016/S1872-2067(14)60288-6 | http://www.sciencedirect.com/science/journal/18722067 | Chin. J. Catal., Vol. 36, No. 4, April 2015

with TiO_2 being widely studied as a photocatalyst because of its nontoxicity, highly chemical stability, and low cost [24,25]. However, TiO_2 has poor solar efficiency (determined by its wide energy band-gap [3.2 eV]) and lower quantum yield (because of the rapid recombination of photo-generated electrons and holes) making practical applications difficult. To enhance the photocatalytic activity of TiO_2, some modifications have been developed, such as doping with metals [26,27] or non-metals [28,29], coupling with other semiconductors [30], and adsorbing organic sensitizers [31,32]. Most recently, Ag_2S was found to be an important photocatalyst and useful in electronic devices because of its large absorption coefficient and a low energy band-gap (0.9–1.05 eV) [33–35]. It has been reported that Ag_2S can catalyze the degradation of methyl orange in the presence of Ag as a co-catalyst under visible light irradiation [36]. Moreover, ternary $Ag/Ag_2S/Ag_3CuS_2$ hollow microspheres have been reported to be more effective when compared with Ag/Ag_2S, Cu_2O, Cu_7S_4 and P25 for the photodegradation of methyl orange under visible light irradiation [37].

In this work, we fabricated two kinds of Ag_xS crystals using hydrothermal (Ag_xS-*H*) and *in situ* ion-exchange (Ag_xS-*IE*) methods. The microstructures and optical properties were investigated by X-ray diffraction (XRD), scanning electron microscopy (SEM), ultraviolet-visible-near infrared (UV-Vis-NIR) absorption spectroscopy, N_2 adsorption-desorption, X-ray photoelectron spectroscopy (XPS) and surface photovoltage (SPV) measurements. The photocatalytic activity and stability of the Ag_xS-*H* were evaluated by the degradation of methyl blue (MB) under visible light irradiation ($\lambda \geq 420$ nm). Ag_xS-*H* showed satisfactory photocatalysis efficiency and good stability, and could be recycled five times without loss of photocatalytic activity.

2. Experimental

2.1. Material preparation

$AgNO_3$, L-cysteine (L-cys), CdS and methyl blue (MB) from the Beijing Chemical Reagent Cooperation (Beijing, China), were analytical grade and used without further purification.

Ag_xS-*H* was prepared by a hydrothermal route. In a typical procedure, 2.7 mmol of $AgNO_3$ was dripped into a solution of 2.7 mmol of L-cysteine in 25 mL of distilled water with continuous stirring over 1 h. The resulting mixture was transferred into a 50-mL Teflon-lined stainless steel autoclave. Then the reactor was sealed and heated to 180 °C for 10 h before being cooled to room temperature. The resulting precipitates were centrifuged and washed using deionized water and absolute ethanol several times, followed by drying at 60 °C for 6 h.

Ag_xS-*IE* was prepared by an *in situ* ion-exchange method. In a typical procedure, CdS (0.5 g) was dispersed in distilled water (50 mL) by ultrasonication for 0.5 h. $AgNO_3$ (1.7 g) was dissolved in distilled water (50 mL) and dripped into the suspension. The mixed suspension was stirred at 70 °C for 12 h. Then, the resulting precipitates were centrifuged and washed with distilled water and absolute ethanol several times, and dried at 60 °C for 6 h.

2.2. Characterization

Powder XRD was performed using a D8 Advance X-ray diffractometer (Bruker, Karlsruhe, Germany) with a Cu K_α source at 40 kV and 40 mA. 2θ scans were performed from 10° to 90° at 4°/min. The morphology of the samples were characterized by field emission scanning electron microscopy (FESEM), which was recorded on a XL30 ESEM microscope (Philips Electronics Co., Eindhoven, Netherlands) operated at a beam energy of 20 kV. UV-Vis-NIR absorption spectroscopy were recorded with a Varian Cary 500 spectrophotometer (Santa Clara, CA, USA), $BaSO_4$ was used as the reference to eliminate background features. The specific surface area of sample was calculated using BET method (Autosorb Quantachrome 1MP, Boynton Beach, FL, USA) based on N_2 adsorption-desorption isomer. XPS (Thermo ESCALAB 250, Waltham, MA, USA) was used to examine the electronic properties of the photocatalysts. The C 1*s* peak at 284.6 eV arising from adventitious carbon was used as the reference. This reference gives binding energy values with precision of ±0.2 eV.

The SPV system contained a source of monochromatic light, a lock-in amplifier (SR830-DSP, Stanford Research Systems, Inc., Sunnyvale, CA, USA) with a light chopper (SR540, Stanford Research Systems, Inc., Sunnyvale, CA, USA), photovoltaic cell, and computer. A 500-W Xe lamp (CHFXQ500 W, Trusttech Co., Inc., Beijing, China) and double-prism monochromator (Zolix SBP500, Beijing, China) provided the monochromatic light. The samples were used as prepared for the SPV measurement, and the contacts between the samples and the indium tin oxide (ITO) electrode were non-ohmic during the measurements of the surface photovoltage. The photovoltaic cell was a sandwich-like structure of ITO-sample-ITO. The powdered sample was placed on the ITO electrode and compressed with another ITO electrode to obtain a film.

2.3. Photocatalytic activity measurement

The photocatalytic performance was evaluated by the degradation of methyl blue (MB) with the photocatalyst (10 mg) suspended in 30 mL of MB solution (10 $mg \cdot L^{-1}$). The reactor was fixed in position, with an irradiated area of 13.8 cm^2. First, the mixed solution was stirred for 30 min in the dark to allow any preliminary adsorption to equilibrate. The photocatalytic reaction was initiated with the visible light irradiation from a 300 W Xe lamp (CEL-HXUV 300, Beijing CHN EDU AuLight Co., Beijing, China). Wavelengths less than 420 nm were removed by an optical filter (UVCUT 420, Beijing CHN EDU AuLight Co., Beijing, China), giving a visible light irradiation region of 420–800 nm. At 20-min intervals, about 500 μL of the reaction mixture was withdrawn, and the composition of the mixture was analyzed after dilution and decantation. The concentration of MB was monitored by UV-Vis spectroscopy via the absorbance of the characteristic peak at 665 nm. These concentrations are denoted *C*, where *C* refers to the concentration of MB at a given interval time and C_{-30} refers to the initial concentration of MB (10 $mg \cdot L^{-1}$) at time −30 min. After the adsorption equilibrium over the Ag_xS-*H* and Ag_xS-*IE* catalysts for 30 min, the

concentration of MB was taken as C_0.

3. Results and discussion

3.1. Characterization of silver sulfide

Two kinds of Ag_xS crystals were prepared by hydrothermal (Ag_xS-*H*) and ionic exchange (Ag_xS-*IE*) methods. As shown in Fig. 1, the diffraction peaks for both Ag_xS-*H* and Ag_xS-*IE* could be indexed as monoclinic Ag_2S (JCPDS 14-0072). The sizes of both the Ag_xS samples estimated from XRD patterns were around 20–30 nm. The morphology and structure of the as-prepared Ag_xS were characterized by SEM, and the images are shown in Fig. 2. The particle sizes were above 100 nm for both the Ag_xS-*H* and Ag_xS-*IE* samples, but the Ag_xS-*H* particles were the smaller. The particle size as observed by SEM is much larger than that calculated from the XRD patterns, because the size obtained from XRD results is crystallite size whereas the particles observed in the SEM images contain many crystallites aggregated together. The larger particle size in the Ag_xS-*IE* sample results in a smaller surface area, as seen by the BET measurement that gave the specific surface areas of Ag_xS-*H* and Ag_xS-*IE* as 2.55 and 1.27 $m^2 \cdot g^{-1}$, respectively. The surface areas for both samples are very small and similar; thus we propose that the surface area or particle size has only a small effect on the photocatalytic activity. The optical properties of Ag_xS were investigated using UV-Vis-NIR techniques (Fig. 3). The spectra of both samples showed a broad absorption covering the entire visible light region, while the absorbance edge of the Ag_xS-*H* sample was shorter than the Ag_xS-*IE* sample, indicating a difference in the electron structure of these two catalysts, which may affect their photocatalytic activity.

To further evaluate the composition, XPS spectra of the Ag_xS were collected as shown in Fig. 4. For the Ag 3*d* spectrum of Ag_xS-*IE*, the peaks at the binding energy of 367.4 and 373.4 eV were assigned to the Ag $3d_{5/2}$ and Ag $3d_{3/2}$ orbitals of Ag^+, and the peaks at 368.0 and 374.0 eV assigned to the Ag $3d_{5/2}$ and Ag $3d_{3/2}$ orbitals of Ag^0 [36]. For Ag_xS-*H*, the Ag^+ peaks were observed at the same binding energies as the above sample, but the Ag^0 peaks were shifted to 368.4 and 374.5 eV. The S 2*p*

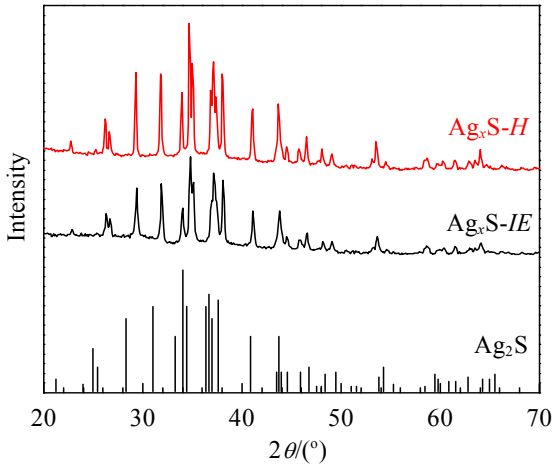

Fig. 1. XRD patterns of Ag_xS-*H* and Ag_xS-*IE*.

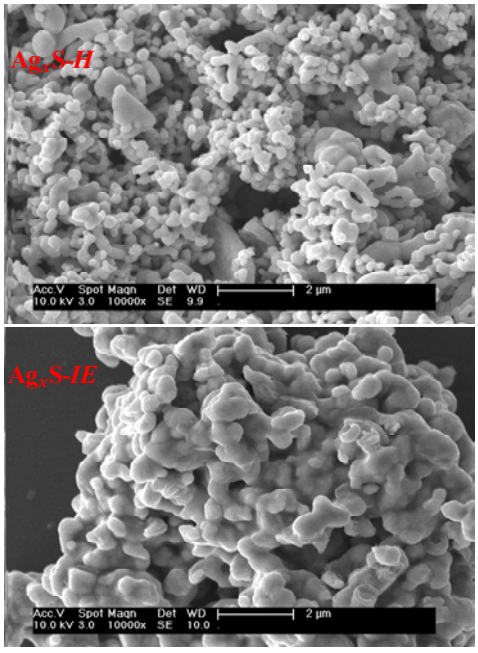

Fig. 2. SEM images of Ag_xS-*H* and Ag_xS-*IE*.

spectra had peaks at the binding energies of 160.1 eV (S $2p_{3/2}$) and 161.3 eV (S $2p_{1/2}$), which were ascribed to monosulphide (S^{2-}) for both Ag_xS-*H* and Ag_xS-*IE*. The peaks around 163.1 eV (S $2p_{3/2}$) and 164.4 eV (S $2p_{1/2}$) for Ag_xS-*IE* were assigned to polysulphides (S_n^{2-}) [38], however, these S_n^{2-} peaks where shifted to 162.5 and 164.0 eV in Ag_xS-*H*. Therefore, differences in the polysulphide species present in both Ag_xS-*H* and Ag_xS-*IE* should affect the electronic structures, which should in turn affect the photocatalytic activities.

3.2. Photocatalytic performance of Ag_xS-*H* and Ag_xS-*IE*

The photocatalytic performances of Ag_xS-*H* and Ag_xS-*IE* were explored in the degradation of MB under visible light irradiation at room temperature. First, the absorptive capacities of the Ag_xS-*H* and Ag_xS-*IE* catalysts were evaluated by keeping the degradation system in the dark for 30 min to achieve an adsorption equilibrium. The degradation reaction was performed under visible light irradiation and, at a given time in-

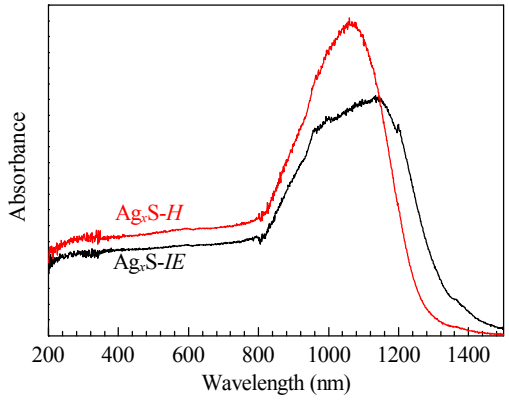

Fig. 3. UV-Vis-NIR absorption spectra of Ag_xS-*H* and Ag_xS-*IE*.

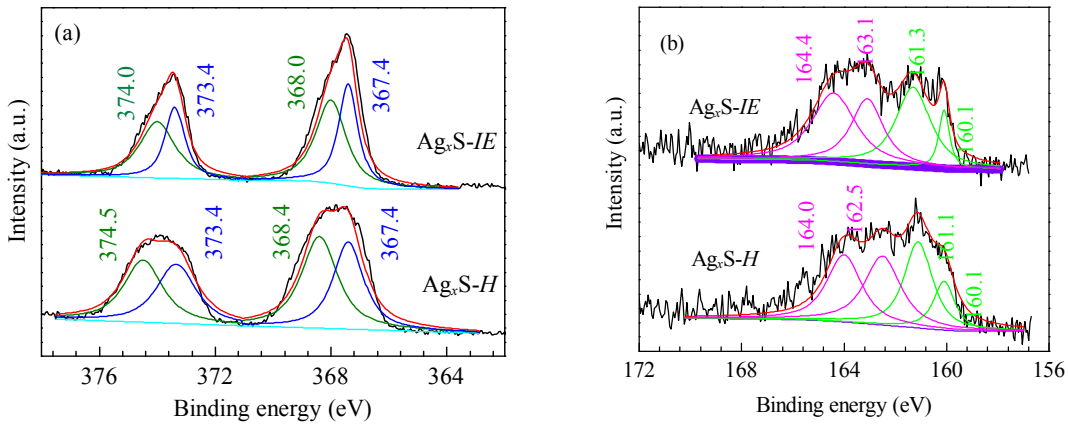

Fig. 4. XPS spectra of Ag 3*d* (a) and S 2*p* (b) of Ag$_x$S-*H* and Ag$_x$S-*IE*.

terval, the concentration of MB was measured by the UV-Vis absorption spectra. The results are shown in Fig. 5(a). Across the effective concentration range of the Lambert–Beer law, the real-time concentration variation of MB (C/C_{-30}, C_{-30} = 10 mg·L^{-1}) is proportional to the normalized absorption value (A/A_{-30}, λ = 665 nm). For comparison, the photocatalytic performance of Ag$_x$S-*IE* was also investigated and is shown in Fig. 5(b). It is clear that both Ag$_x$S-*H* and Ag$_x$S-*IE* exhibited excellent photocatalytic activity in the degradation of MB. Moreover, the photocatalytic activity of Ag$_x$S-*H* was much higher than that of Ag$_x$S-*IE*. This may be ascribed to the wider band gap and the weaker recombination of photoinduced charges which should be the most important factor in the photocatalytic efficiency, which is discussed further in Section 3.4.

Furthermore, when we prolonged the reaction time, the photocatalytic efficiency (C/C_{-30}) of MB over Ag$_x$S-*H* reached 99% at 2 h. Moreover, the bulk solution at this time was completely colorless or transparent. To confirm the degree of mineralization, the final products were identified by high-performance liquid chromatography-mass spectroscopy (HPLC-MS). There was almost no MB, and no organic molecule or organic intermediates were detected, when comparing with pure MB, indicating MB had been degraded into inorganic compounds.

Generally, the photocatalytic oxidation of organic dye pollutants follows first-order kinetics which can be expressed as follows: $\ln(C_0/C) = k_{app}\cdot t$, where k_{app} is the apparent rate constant (min^{-1}), C_0 is the concentration of MB after the absorption equilibrium for 30 min (mg·L^{-1}), and C is the concentration at a given reaction time interval (mg·L^{-1}). According to Fig. 5(b), the reaction followed first-order kinetics. A linear relationship between $\ln(C_0/C)$ and reaction time is shown in Fig. 6(a), confirming the degradation of MB over Ag$_x$S-*H* follows first order kinetics. For the degradation of MB, the apparent rate constant k_{app} was calculated and shown in Fig. 6(b). The k_{app} for Ag$_x$S-*H* is 2.63 × 10^{-2} min^{-1}, and this is larger than the k_{app} of Ag$_x$S-*IE* (1.44 × 10^{-2} min^{-1}).

3.3. *Reusability of Ag$_x$S-H*

Stability is a greatly important factor when considering a heterogeneous catalyst for a practical application. In general, metal sulfide compounds suffer from photocorrosion, as the material is oxidized by its own photogenerated holes ($M_2S_x + h^+ \rightarrow M_x^+ + S$), especially in aqueous solution [39,40]. Here, the photostability of Ag$_x$S-*H* was checked in the degradation of MB under visible light irradiation. After first run, the catalyst was separated by centrifugation at 12000 r/min, washed three times with distilled water, and reused in the next run. The re-

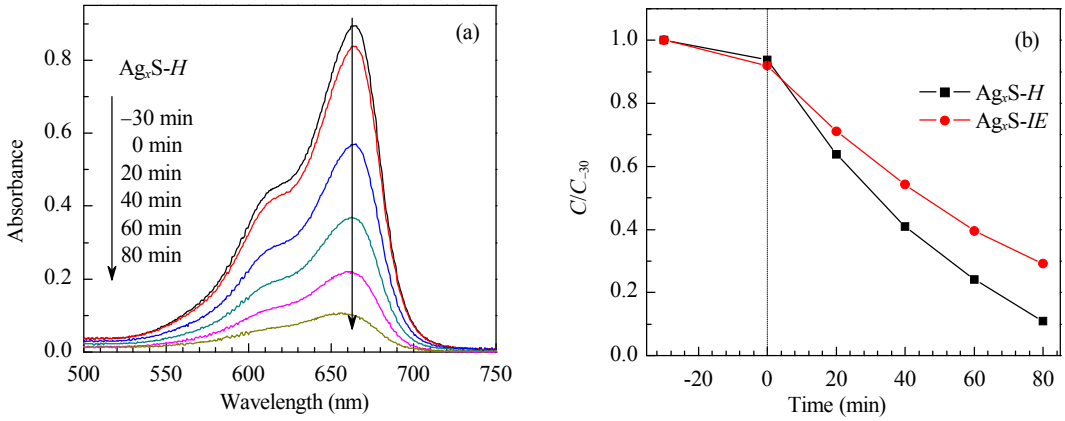

Fig. 5. (a) UV-Vis absorbance spectra of MB over Ag$_x$S-*H* at different reaction intervals; (b) Photocatalytic performance of Ag$_x$S-*H* and Ag$_x$S-*IE* in the degradation of MB under visible light irradiation at room temperature.

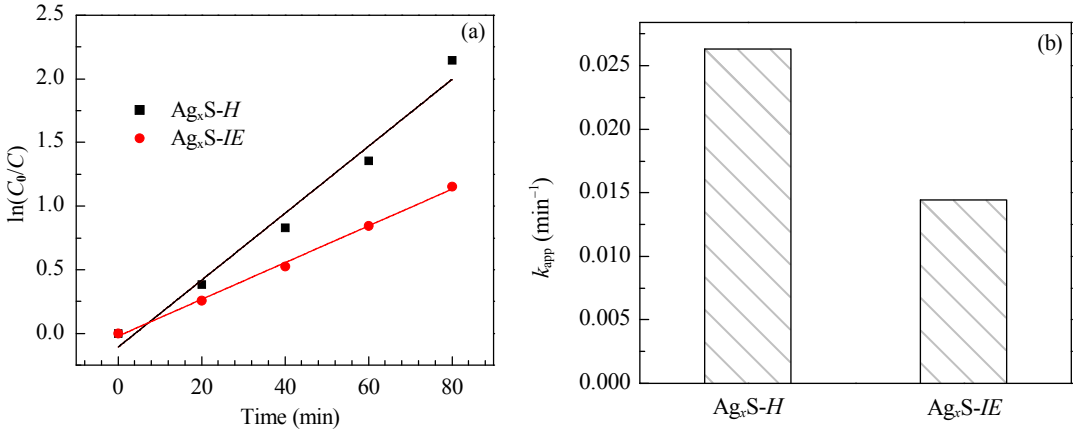

Fig. 6. The kinetic curves (a) and estimated k_{app} (b) for the degradation of MB over different photocatalysts.

sults are shown in Fig. 7(a). The photocatalytic efficiency (C/C_0) was 89% for the first run, and was still 86.7% for the fifth run, indicating that the photocatalytic activity of Ag$_x$S-*H* was quite stable without obvious decrease during recycling. Fig. 7(b) presents the XRD patterns of the fresh and used Ag$_x$S-*H* photocatalyst. The crystal phase and the structure of Ag$_x$S-*H* did not change after five runs, indicating that the Ag$_x$S crystal is stable during the photocatalytic degradation process.

3.4. Proposed mechanism of the photocatalytic degradative process

The band edge positions of photocatalysts are of particular importance in the photocatalytic reaction. In the present work, the band edge potentials of the catalysts were estimated using an equation related to the Mulliken electronegativity. Here, the electronegativity (*EE*) of an atom is the arithmetic mean of the atomic electron affinity (*EA*) and the first ionization energy (*IE*) [41]. The CB edge position of an uncharged semiconductor can be calculated according to the empirical equation [41,42]: $E_{CB} = \chi - E^e - 0.5\ E_g$, where E_{CB} is the CB edge potential, χ is the electronegativity of the semiconductor (*SE*, the geometric mean of the electronegativity of the constituent atoms), E^e is the energy of free electrons on the hydrogen scale (~4.5 eV), E_g is the band gap energy of the semiconductor, which was determined by the Tauc equation ($ahv = A(hv - E_g)^n$), where a is the absorption coefficient measured as a function of photon energy hv, and A is a constant factor determined by the transition probability), and n is a number that depends on the type of transition. The transitions of Ag_2S are allowed and direct, which means the Tauc equation requires $n = 1/2$ for each material. Therefore, a straight-line fit of a plot of $(ahv)^2$ versus hv gives the Tauc equation, as shown in Fig. 8. The hv value at the intersection of the tangent line and the horizontal axis is the band gap E_g [43]. The band gap is affected by the crystallite size, phase transition, and semiconductor components. The crystallite sizes in Ag$_x$S-*H* and Ag$_x$S-*IE* were similar (20–30 nm), and much bigger than the Bohr exciton radius of this material (~2.2 nm) [44], so the crystallite size will only have a small effect on the band gap. Phase transitions in crystals can change the band gap. It has been reported that a series of structural phase transitions of Ag_2S can induce noticeable changes in electrical transport parameters, resulting in the change of the band gap of Ag_2S [45]. However, the XRD patterns reported here for both Ag$_x$S-*H* and Ag$_x$S-*IE* were similar, indicating the two samples had the same phase, which means they should have very similar band gaps. In contrast, nonstoichiometric semiconductors may have different band gap structures compared with the stoichiometric equivalent material [46,47]. The band gap of reduced TiO_2 has been reported to be narrower than that of the bulk TiO_2, with a

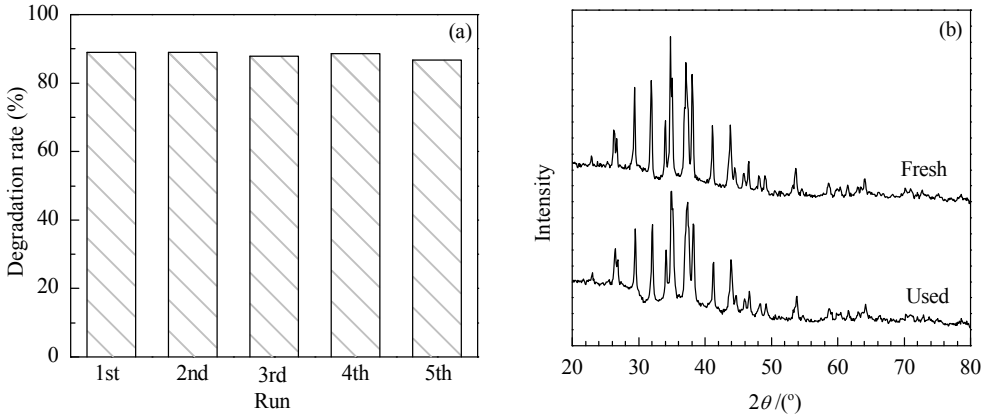

Fig. 7. (a) The recycling results of Ag$_x$S-*H* in the photodegradation of MB; (b) XRD patterns of the fresh and used Ag$_x$S-*H* after five runs.

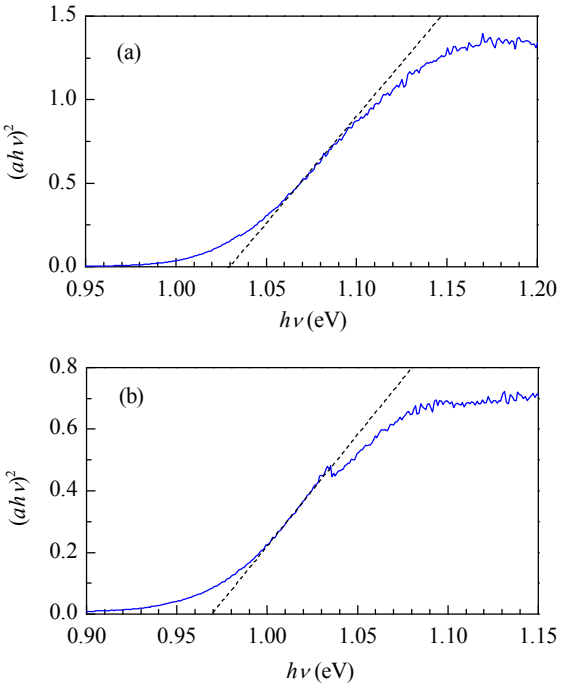

Fig. 8. Tauc's plot for Ag_xS-*H* (a) and Ag_xS-*IE* (b).

miniband appearing just below the bottom of the conducting band and the width of this band is related to the concentration of the Ti^{3+} or oxygen vacancy [46]. The Ag:S mole ratio of both Ag_xS-*H* and Ag_xS-*IE* were estimated by ICP measurement as 0.87 and 1.24, respectively, which is much lower than the stoichiometric ratio of bulk Ag_2S. This difference in the Ag:S mole ratio is large enough to be significant and may well affect the band gap. The effect of the Ag:S mole ratio is very complicated and it is being studied further in our lab. The Ag_xS-*H* and Ag_xS-*IE* samples have E_g of 1.03 and 0.97 eV, respectively, which are larger than the bandgap of Ag_2S (0.92 eV). The Ag:S ratio less than 2 is most likely because of the existence of polysulphide species in these samples. The VB edge potential (E_{VB}) can be determined using $E_{VB} = E_{CB} + E_g$. The CB and VB potentials determine the samples' reductive and oxidative ability [48]. Based on the above equations, the E_{CB} and E_{VB} were calculated, and the results are listed in Table 1. E_{CB} was more cathodic for Ag_xS-*H* (0.23 eV), while E_{VB} (1.26 eV) was more anodic when compared with Ag_xS-*IE*, for which the E_{CB} was 0.26 eV and the E_{VB} was 1.23 eV. Therefore, Ag_xS-*H* is a stronger reducing agent when forming superoxide ions ($\bullet O^{2-}$). Moreover, the photogenerated holes of Ag_xS-*H* are more able to oxidize MB when compared with Ag_xS-*IE* [37]. Consequently,

Table 1
Band energies calculated for Ag_xS-*H* and Ag_xS-*IE* from data in Fig. 7.

CE	*EA* (eV)	*IE* (eV)	*EE* (eV)	*SE* (eV)	Catalyst	E_g (eV)	E_{CB} (eV)	E_{VB} (eV)
Ag	2.00	7.59	4.80	5.24	Ag_xS-*H*	1.03	0.23	1.26
S	2.08	10.38	6.23		Ag_xS-*IE*	0.97	0.26	1.23

CE: Constituent elements; *EA*: Electron affinity; *IE*: Ionization energy; *EE*: Element electronegativity; *SE*: Semiconductor electronegativity; E_g: band gap energy; E_{CB}: conduction band edge potential; E_{VB}: valence band edge potential.

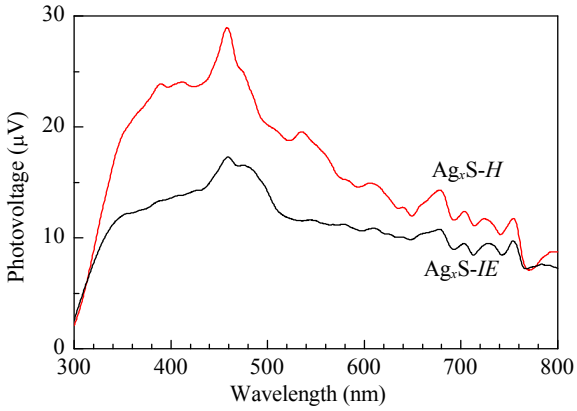

Fig. 9. Surface photovoltage spectra of samples.

Ag_xS-*H* exhibited the higher photocatalytic efficiency than Ag_xS-*IE* in the degradation of MB.

The transfer behavior of the photoinduced charge carriers was investigated by SPV measurements. The photovoltic signal represents the difference in the surface potential barriers before and after illumination, which in turn is caused by the separation of photoinduced charge carriers. Therefore, the strength of the SPV signal determines the amount of light absorbed and the transport of excess carriers in a semiconducting material [49–51]. Fig. 9 displays the SPV spectra of the samples. Each sample showed a positive signal in the range of 300–800 nm, with Ag_xS-*H* exhibiting a much stronger SPV response. This suggested that the light absorbing region of the two catalysts is the same, and that the photoinduced electrons migrate from the surface to the bulk and the photoinduced holes move to the surface forming better separated exciton pairs in Ag_xS-*H*. This means that the recombination of electro-hole pairs of Ag_xS-*H* is weaker than in Ag_xS-*IE*, leading to enhanced photocatalytic activity.

Based on the above analysis, a possible pathway for the degradation of MB over Ag_xS has been proposed. As shown in Scheme 1, the present MB degradation over Ag_xS under the visible light irradiation is mainly because of oxidation of MB with •OH, which is produced from water or oxygen, and partly because of electron holes generated in Ag_xS. This is in agreement with the literature, where Ganguli et al. [52] discussed the photodegradation process of MB over ZnO/Ag_2S with various active species scavengers and electron paramagnetic resonance

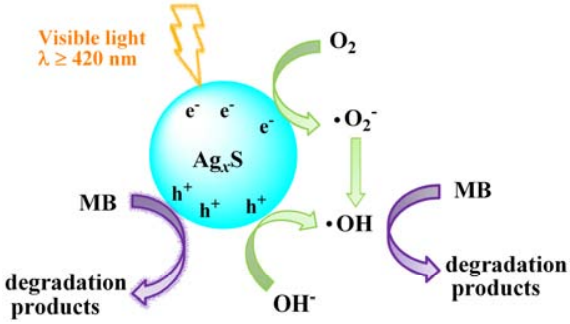

Scheme 1. Possible photocatalytic mechanism for Ag_xS under visible light irradiation.

spectroscopy, they analyzed the active species such as hydroxyl radicals (•OH), electrons (e^-), holes (h^+), and superoxide radical anions ($•O_2^-$). They concluded that the MB oxidation proceeded mainly through the reaction with •OH, and partly via the generated electron holes (h^+).

4. Conclusions

The Ag_xS-*H* crystals fabricated by a hydrothermal method was found to be more efficient in the photocatalysis of MB degradation under visible light irradiation, because it has a wider band gap and weaker recombination of photoinduced charges than Ag_xS-*IE,* prepared by *in-situ* ion-exchange. Ag_xS-*H* exhibited high stability, remaining active after being reused five times. The hydroxyl radicals appear to be the key factor in the photo-degradation of MB over Ag_xS under visible light irradiation. The Ag_xS crystals developed in this work have potential applications in the treatment or degradation of organic dyes by exposing the wastewater to sunlight.

Acknowledgments

We thank Prof. Tengfeng Xie from Jilin University for the helps in surface photovoltage measurements and Prof. Yihang Guo from Northeast Normal University for the helps in UV-Vis-NIR absorption spectra measurements.

References

[1] Hou Y, Li X Y, Zhao Q D, Chen G H, Raston C L. *Environ Sci Technol*, 2012, 46: 4042
[2] Shannon M A, Bohn P W, Elimelech M, Georgiadis J G, Marinas B J, Mayes A M. *Nature*, 2008, 452: 301
[3] Meshko V, Markovska L, Mincheva M, Rodrigues A E. *Water Res*, 2001, 35: 3357
[4] Cooper P. *J Soc Dyers Colour*, 1993, 109: 97
[5] Patil S S, Shinde V M. *Environ Sci Technol*, 1988, 22: 1160
[6] Moore A T, Vira A, Fogel S. *Environ Sci Technol*, 1989, 23:403
[7] Correia V M, Stephenson T, Judd S J. *Environ Technol*, 1994, 15: 917
[8] Arslan I, Balcioglu I A. *Dyes Pigments*, 1999, 43: 95
[9] Wu F, Deng N S, Zuo Y G. *Chemosphere*, 1999, 39: 2079
[10] Kang S F, Liao C H, Po S T. *Chemosphere*, 2000, 41: 1287
[11] Balanosky E, Fernandez J, Kiwi J, Lopez A. *Water Sci Technol*, 1999, 40: 417
[12] Arslan I, Balcioglu I A, Tuhkanen T. *Environ Technol*, 1999, 20: 921
[13] Ince N H, Gonenc D T. *Environ Technol*, 1997, 18: 179
[14] Kuo W S, Ho P H. *Chemosphere*, 2001, 45: 77
[15] Zhang F L, Zhao J C, Shen T, Hidaka H, Pelizzetti E, Serpone N. *Appl Catal B*, 1998, 15: 147
[16] Qu P, Zhao J C, Shen T, Hidaka H. *J Mol Catal A*, 1998, 129: 257
[17] Galindo C, Jacques P, Kalt A. *Chemosphere*, 2001, 45: 997
[18] Tang W Z, An H. *Chemosphere*, 1995, 31: 4157
[19] Konstantinou I K, Albanis T A. *Appl Catal B*, 2004, 49: 1
[20] Pelaez M, Nolan N T, Pillai S C, Seery M K, Falaras P, Kontos A G, Dunlop P S M, Hamilton J W J, Byrne J A, O'Shea K, Entezari M H, Dionysiou D D. *Appl Catal B*, 2012, 125: 331
[21] Chong M N, Jin B, Chow C W K, Saint C. *Water Res*, 2010, 44: 2997
[22] Wu P G, Xie R C, Imlay J A, Shang J K. *Appl Catal B*, 2009, 88: 576
[23] Rizzo L, Sannino D, Vaiano V, Sacco O, Scarpa A, Pietrogiacomi D. *Appl Catal B*, 2014, 144:369
[24] Chen X, Mao S S. *Chem Rev*, 2007, 107: 2891
[25] Fujishima A, Rao T N, Tryk D A. *J Photochem Photobiol C*, 2000, 1: 1
[26] Tong T Z, Zhang J L, Tian B Z, Chen F, He D N. *J Hazard Mater*, 2008, 155: 572
[27] Tian B Z, Li C Z, Gu F, Jiang H B, Hu Y J, Zhang J L. *Chem Eng J*, 2009, 151: 220
[28] Asahi R, Morikawa T, Ohwaki T, Aoki K, Taga Y. *Science*, 2001, 293: 269
[29] Niu Y X, Xing M Y, Tian B Z, Zhang J L. *Appl Catal B*, 2012, 115: 253
[30] Zhao W, Ma W H, Chen C C, Zhao J C, Shuai Z G. *J Am Chem Soc*, 2004, 126: 4782
[31] Bae E Y, Choi W Y, Park J W, Shin H S, Kim S B, Lee J S. *J Phy Chem B*, 2004, 108: 14093
[32] Zou W W, Zhang J L, Chen F. *Mater Lett*, 2010, 64: 1710
[33] Xie Y, Heo S H, Kim Y N, Yoo S H, Cho S O. *Nanotechnology*, 2010, 21: 015703
[34] Neves M C, Nogueira J M F, Trindade T, Mendonca M H, Pereira M I, Monteiro O C. *J Photochem Photobiol A*, 2009, 204: 168
[35] Hwang I, Seol M, Kim H, Yong K. *Appl Phys Lett*, 2013, 103: 023902
[36] Yang W L, Zhang L, Hu Y, Zhong Y J, Wu H B, Lou X W. *Angew Chem Int Ed*, 2012, 51: 11501
[37] Xing C S, Zhang Y, Wu Z D, Jiang D L, Chen M. *Dalton Trans*, 2014, 43: 2772
[38] Smart R S C, Skinner W M, Gerson A R. *Surf Interface Anal*, 1999,

Graphical Abstract

Chin. J. Catal., 2015, 36: 564–571 doi: 10.1016/S1872-2067(14)60288-6

A stable and active Ag_xS crystal preparation and its performance as photocatalyst

Pingjing Chang, Haiyang Cheng*, Weiwei Lin, Xiaoru Li, Fengyu Zhao*
Changchun Institute of Applied Chemistry, Chinese Academy of Sciences; University of Chinese Academy of Sciences

Ag_xS exhibits efficient photocatalytic activity in the degradation of MB under visible light irradiation; MB was oxidized mainly by the hydroxyl radicals and partly via electron holes generated in the Ag_xS.

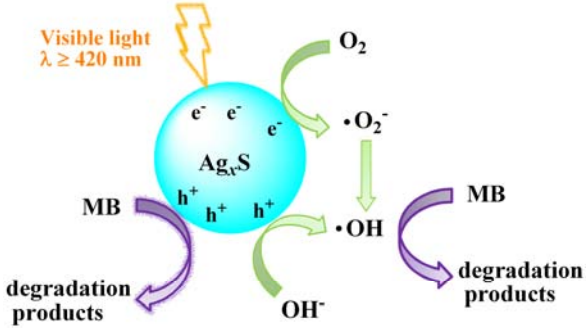

28:101
[39] Chen Z, Liu S Q, Yang M Q, Xu Y J. *ACS Appl Mater Interfaces*, 2013, 5: 4309
[40] Bao N Z, Shen L M, Takata T, Domen K. *Chem Mater*, 2008, 20: 110
[41] Butler M A, Ginley D S. *J Electrochem Soc*, 1978, 125: 228
[42] Netherco A H. *Phys Rev Lett*, 1974, 33: 1088
[43] Huxter V M, Mirkovic T, Nair P S, Scholes G D. *Adv Mater*, 2008, 20: 2439
[44] Zhang Y J,Liu Y S, Li C Y, Chen X Y, Wang Q B. *J Phys Chem C*, 2014, 118: 4918
[45] Zhang J K, Liu C L, Zhang X, Ke F, Han Y H, Peng G, Ma Y Z, Gao C X. *Appl Phys Lett*, 2013, 103: 082116
[46] Zuo F, Wang L, Wu T, Zhang Z Y, Borchardt D, Feng P Y. *J Am Chem Soc*, 2010, 132: 11856
[47] Wang H K, Dou K P, Teoh W Y, Zhan Y W, Hung T F, Zhang F H, Xu J Q, Zhang R Q, Rogach A L. *Adv Funct Mater*, 2013, 23: 4847
[48] Hagfeldt A, Gratzel M. *Chem Rev*, 1995, 95: 49
[49] Zhang X, Zhang L Z, Xie T F, Wang D J. *J Phys Chem C*, 2009, 113: 7371
[50] Gross D, Mora-Seró I, Dittrich T, Belaidi A, Mauser C, Houtepen A J, Da Como E, Rogach A L, Feldmann J. *J Am Chem Soc*, 2010, 132: 5981
[51] Fan H M, Jiang T F, Li H Y, Wang D J, Wang L L, Zhai J L, He D Q, Wang P, Xie T F. *J Phys Chem C*, 2012, 116: 2425
[52] Khanchandani S, Srivastava P K, Kumar S, Ghosh S, Ganguli A K. *Inorg Chem*, 2014, 53: 8902

高效稳定的Ag_xS的制备及其光催化性能

常平静[a,b,c], 程海洋[a,b,#], 林伟伟[a,b], 李小汝[a,b,c], 赵凤玉[a,b,*]
[a]中国科学院长春应用化学研究所, 电分析化学国家重点实验室, 吉林长春130022
[b]中国科学院长春应用化学研究所, 绿色化学与过程实验室, 吉林长春130022
[c]中国科学院大学, 北京100049

摘要: 分别采用水热法(Ag_xS-*H*)和原位离子交换法(Ag_xS-*IE*)制备了Ag_xS. 采用扫描电镜(SEM)、X射线衍射光谱、紫外可见近红外吸收光谱、N_2吸附-脱附、X射线光电子能谱和表面光电压测试对催化剂进行了表征. 以光($\lambda \geq 420$ nm)降解亚甲基蓝为模型反应, 考察了Ag_xS的光催化性能. 与Ag_xS-*IE*相比, Ag_xS-*H*具有较小的粒径、较大的禁带宽度、较低光生电荷复合率, 因此具有较高的光催化活性. 此外, Ag_xS-*H*还表现了较好的稳定性, 循环使用五次仍能够保持较高的光催化活性. 结果表明, Ag_xS光催化降解亚甲基蓝主要以羟基自由基氧化为主, 光生空穴氧化为辅的光催化氧化过程. Ag_xS-*H*作为一种有效的光催化剂, 在降解有机染料污水方面具有潜在的应用价值.

关键词: Ag_xS; 可见光照射; 光催化降解反应; 有机污染物; 禁带宽度

收稿日期: 2014-11-23. 接受日期: 2015-01-08. 出版日期: 2015-04-20.
*通讯联系人. 电话/传真: (0431)85262410; 电子信箱: zhaofy@ciac.ac.cn
#通讯联系人. 电话/传真: (0431)85262454; 电子信箱: hycyl@ciac.ac.cn
基金来源: 国家自然科学基金(21273222).
本文的英文电子版由Elsevier出版社在ScienceDirect上出版(http://www.sciencedirect.com/science/journal/18722067).